

Fermi National Accelerator Laboratory

FERMILAB-Pub-91/19
[SSCL-277]

Effects from Measured Ground Motions at the SSC

King-Yuen Ng
Fermi National Accelerator Laboratory
P.O. Box 500
Batavia, Illinois 60510

Jack M. Peterson
Superconducting Super Collider Laboratory
2550 Beckleymeade Ave
Dallas, Texas 75237

December 1990



Operated by Universities Research Association Inc. under contract with the United States Department of Energy

EFFECTS FROM MEASURED GROUND MOTIONS AT THE SSC

King-Yuen Ng

Fermi National Accelerator Laboratory[†]
P.O. Box 500
Batavia, IL 60510

Jack M. Peterson

Superconducting Super Collider Laboratory*
2550 Beckleymeade Ave.
Dallas, TX 75237

December 1990

[†]Operated for the U.S. Department of Energy under Contract No. DE-AC02-76CHO3000.

*Operated by University Research Association, Inc., for the U.S. Department of Energy under Contract No. DE-AC02-89ER40486.

EFFECTS FROM MEASURED GROUND MOTIONS AT THE SSC*

King-Yuen Ng

Fermi National Accelerator Laboratory
P.O. Box 500
Batavia, IL 60510

and

Jack M. Peterson

Superconducting Super Collider Laboratory[†]
2550 Beckleymeade Avenue
Dallas, TX 75237

December 1990

Abstract

The separation of the two beams in the SSC caused by ground motion produced by railroad and highway traffic crossing over the ring and by nearby quarry blasts were estimated from measured amplitude spectra using a complete optical model of the accelerator lattice, but a simplified model of the ground structure. The beam separation expected from the largest ground motion recorded from train crossings is only a few percent of the rms beam width at the beam-crossing points. However, the beam separation caused by quarry blasts are larger and can momentarily produce significant loss in luminosity.

* This work is supported by the U.S. Department of Energy under Contract No. DE-AC02-76CH03000.

[†] Operated by the Universities Research Association, Inc., for the U.S. Department of Energy under Contract No. DE-AC02-89ER40486.

1. INTRODUCTION

Movement of the quadrupole magnets in the Superconducting Super Collider (SSC) affect the closed orbits of the two proton beams differently and so can cause the two beams to separate from each other at the crossing points in the interaction regions. The theory of these effects was developed in SSC-212 (FN-511)¹.

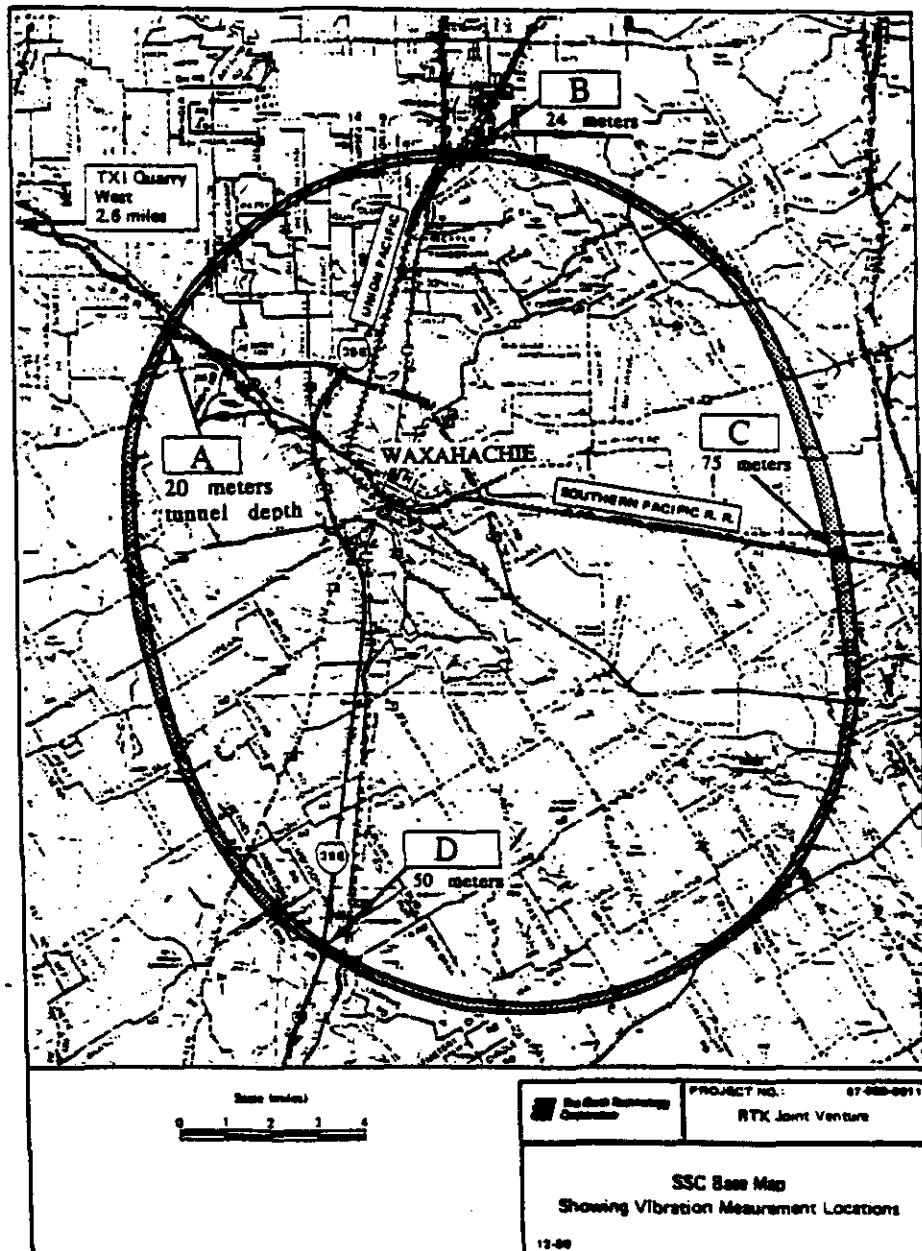
Recently, measurements were made of the ground motion at the planned site of the SSC by K. Hennon and D. Hennon of the Earth Technology Corporation². This document is a report on the impact of these data on the projected operation of the SSC.

2. GROUND MOTION MEASUREMENTS

2.1 Experimental Method

The geophone measurements were made at 5 points where railroads and/or highways cross over the ring, as shown in Figure 1. At these points measurements were made of the ambient vibration levels and of the levels due to trains and to highway traffic and to blasts from a nearby quarry. Several sets of data were usually taken in each bore-hole, near the surface, and near the top of the Austin chalk stratum, and at the projected depth of the SSC tunnel, most of which is in the Austin chalk. Additional data were made at several depths of the ground motion produced by hammer blows at the surface in order to measure the down-hole velocity of the ground waves as a function of depth at each site. The projected tunnel depths at the 5 measurement sites ranged from 20 to 75 meters.

Two types of geophones were employed. The first type was a triaxial array of geophones (Mark Products model L-10-3WD) that were sensitive to vibration velocity mainly at frequencies above 20 Hz. The data from these geophones showed that the ground motion due to trains was predominantly in the vertical direction. The principal quantitative data came from single vertical-direction geophones (Mark Products model L-4C). Their response curves were substan-



NOTE : Two bore-holes, one near the railroad crossing and one 320 meters to the southeast, were used at Site B. Measurements were made near the surface, near the top of the Austin chalk layer, and at the anticipated tunnel depth (indicated at each measuring site).

Figure 1. Ground-motion Measurements in Bore-holes at Sites A, B, C, and D.

tially flat at 4.2 volts per inch/sec for frequencies from 1.5 Hz to 200 Hz and fell to about one-half the plateau value at about 0.75 Hz.

The output signal from each geophone was recorded and analyzed on a Hewlett Packard model HP-3562A Dynamic Signal Analyzer. A four-second interval of the largest recorded signal at tunnel depth due to a train passing overhead is shown in Figure 2. The corresponding displacement spectrum obtained by fast Fourier transform and application of the measured frequency response of the geophone used plus time integration to convert velocity to displacement is shown in Figure 3.

A similar sample of the signal produced by a relatively large amount of high explosive (4,243 pounds) at a quarry located 9.4 km northwest of the measuring site A (see Figure 1) is shown in Figure 4. The corresponding amplitude spectrum is shown in Figure 5.

2.2 Experimental Results

2.2.1 Properties of the Propagating Medium. From the measured down-hole velocities of the longitudinal (compressional) and transverse (shear) waves, plus

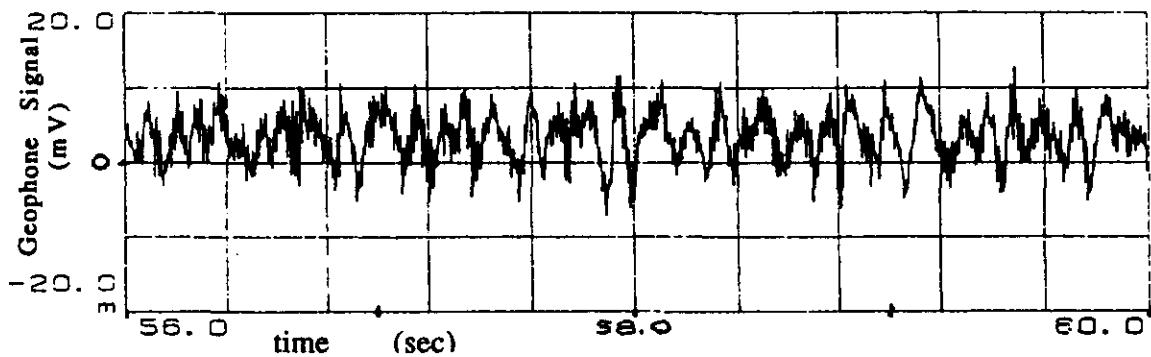


Figure 2. Signal from Geophone at Tunnel Depth (20 meters) due to a Train Crossing Overhead at Site A in the Northwest Arc of the SSC. This was the largest of the 17 train signals recorded.

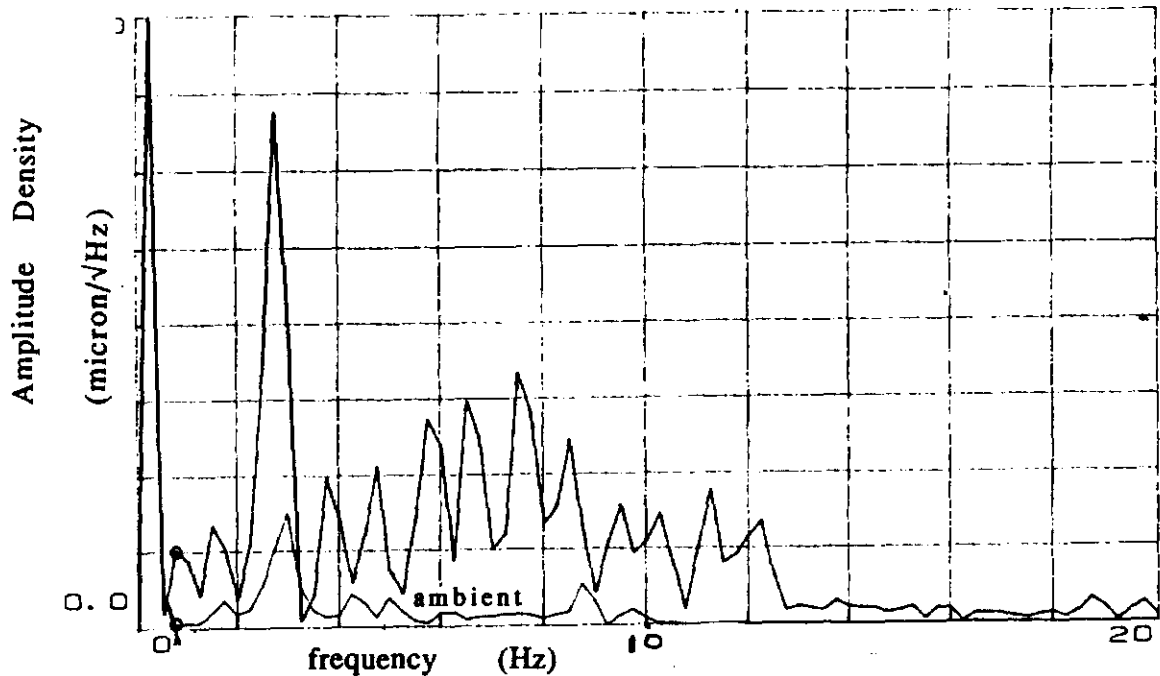


Figure 3. The Vibration Amplitude Spectrum Obtained by a Fast Fourier Transform of the Signal in Figure 2, Application of the Measured Geophone Calibration Curve, and Time-integration to Convert the Velocity Spectrum to a Displacement Spectrum. The units ($\text{m}/\sqrt{\text{Hz}}$) are due to the power-spectrum analysis that was employed—i.e., the square of the geophone signal was frequency analyzed.

the measured material densities, the elastic constants, the Poisson ratio, and the velocity of dominant Rayleigh ground waves in the Austin chalk can be inferred. These results varied considerably from bore-hole to bore-hole and with depth in each bore-hole, as shown in Table 1. The corresponding results from the one bore-hole in the Taylor marl formation (on the east side of the SSC ring) were compatible with those from the Austin chalk stratum.

2.2.2 Measured Ground-Wave Displacements. The largest measured ground displacement due to train traffic were recorded in the bore-hole in the northwest arc, where the minimum tunnel depth occurs (about 20 meters). Figures 2 and 3

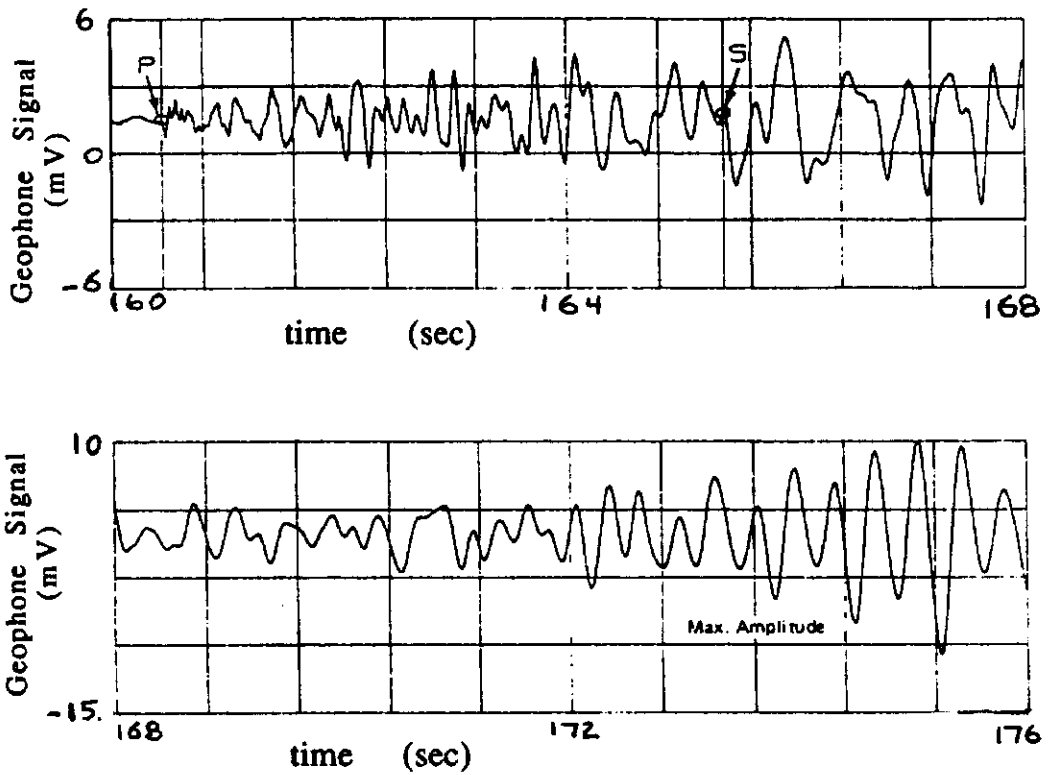


Figure 4. Geophone Signal due to a Quarry Blast Recorded at Tunnel Depth, Site A, in the Northwest Arc. The arrival times of the *P*- and *S*-waves are marked. The quarry is located about 9.4 km to the northwest, near Midlothian.

Table 1. Results from Down-Hole and Quarry Blast Velocity Measurements in the Austin Chalk Stratum (density 2.16 gm-cm^{-3})

Location	Velocities (m/s)			Poisson ratio	Elastic Moduli ($\times 10^5$ psi)	
	longitud.	transv.	Rayleigh		Young's	shear
Near top of stratum	1100-1500	625-885	580-810	0.17-0.36	3.1-5.7	1.2-2.5
Near tunnel depth	1700-2700	1000-1550	900-1450	0.25-0.35	7.9-19.0	3.2-7.6
From blast data	3260	1400	1300	0.39	16.7	6.0

show the raw geophone signal and the corresponding displacement spectrum. All of the train spectra were similar, being characterized typically by a narrow peak near 2 or 3 Hz plus a broad maximum centered in the 6 to 10 Hz range. The displacement spectrum in Figure 3 was simply integrated to produce an approximate vertical ground motion amplitude of 0.55 micron in the 3-Hz component and a 0.58 micron amplitude at about 7 Hz. (The phase information required for a Fourier reconstruction of the original time-dependent ground-motion wave form was not available.) These component amplitudes compare well with the maximum amplitude of 1.1 micron obtained from integrating the original geophone signal and applying the average geophone calibration constant, as shown in Figure 6.

The ground motion caused by automobile and truck traffic on Interstate Highway 35-E where it crosses the south arc of the SSC (about 50 meters above the tunnel) was much less than that from the train crossings. The largest recorded amplitude due to highway traffic was only 0.03 micron at tunnel depth, the dominant frequency being about 18 Hz.

The largest recorded geophone signal due to a quarry blast was shown in Figure 4 and the corresponding displacement spectrum in Figure 5. The displacement peak near 1 Hz when integrated gives an amplitude of approximately 1.4 micron for that frequency component, and that near 3 Hz gives an amplitude of about 1.1 micron.

2.2.3 Ground Wave Attenuation. The attenuation characteristics of ground waves at the SSC site were estimated in three ways:

(1) From the time profile of the geophone signal at tunnel depth due to an approaching train: The train distance at which the geophone signal became apparent relative to the ambient noise signal (typically 2 or 3 percent of that when the train crossed overhead) was fitted to a computational model (to be described in Section 3), assuming attenuation of the form $e^{-\alpha R}$, with α expressed as $\alpha = f/L_c$, where L_c is the characteristic attenuation length at $f = 1$ Hz. These data resulted in values of the characteristic attenuation length ranging from 0.7 to 2.5 km, with the best data favoring a value near 1.0 km.

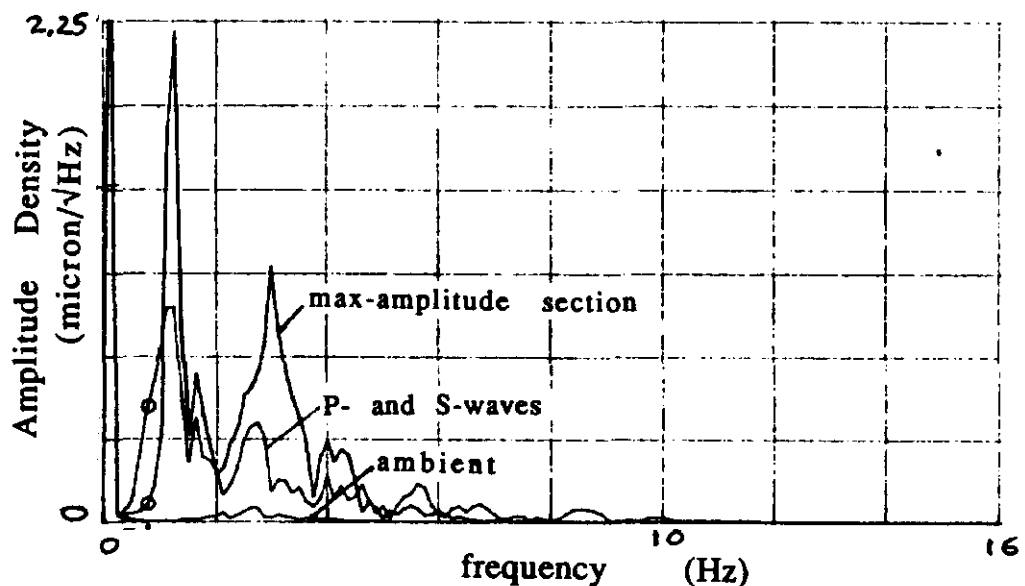


Figure 5. The Amplitude Spectrum Corresponding to the Geophone Signal in Figure 4.

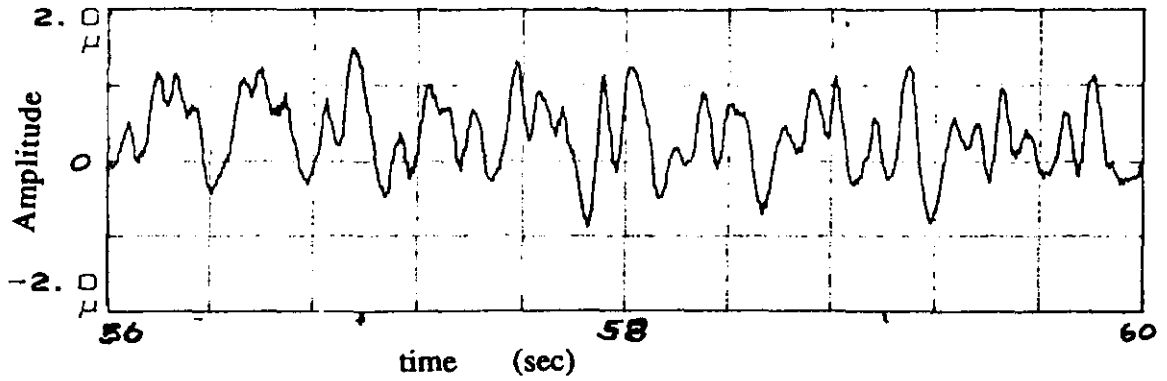


Figure 6. The Approximate Displacement Waveform Obtained by Integrating the Geophone Signal of Figure 2 and Applying the Average Geophone Calibration Constant.

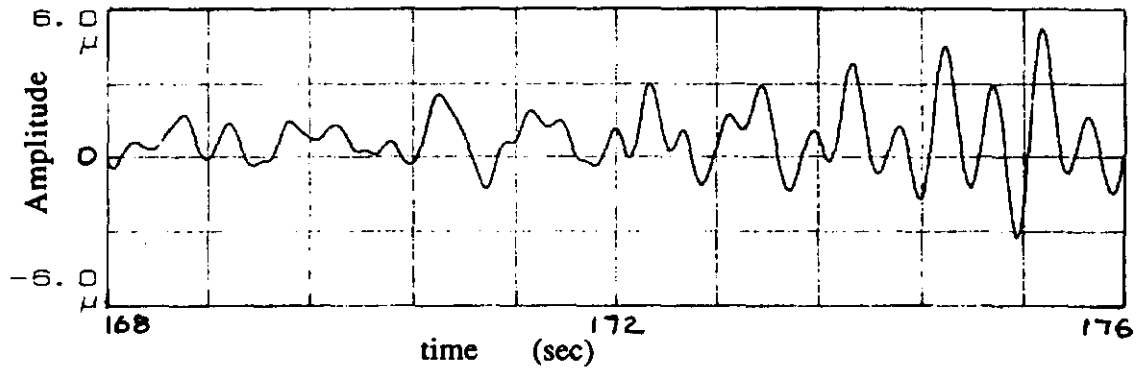


Figure 7. The Approximate Displacement Waveform Obtained by Integrating the Geophone Signal of Figure 4 and Applying the Average Geophone Calibration Constant.

(2) From simultaneous measurements of train-induced ground waves at tunnel depth in two separate bore-holes, one directly below the train crossing at the B site in Figure 1 and the other some 200 meters to the side: Fitting these data to the computational train model resulted in a characteristic attenuation length of about 5 km/Hz.

(3) From measurement of the relative amplitudes of the ground waves due to a quarry blast at two well-separated sites: One pair of geophone sites (at tunnel depth) were sites A and B on Figure 1, which are 9.4 and 19.5 km, respectively, from the quarry. The second pair were sites A and C, which are 9.4 and 33.4 km from the quarry. The characteristic attenuation length that best fit these data was 10 km/Hz.

The shorter attenuation lengths obtained from the train data is interpreted as due partly to the greater absorption in the relatively soft alluvial deposits in which the railroad tracks are imbedded and partly to the reflections of the ground waves at the alluvial/Austin-chalk interface. Differing effective thicknesses of the alluvial deposits could account for the different attenuation lengths derived from the (1) and (2) types of data described above. The longer attenuation length obtained from the blast data is understandable in that the high-explosive blasts occurred in the relatively hard Austin-chalk layer itself, so that both absorptive losses and reflective losses are less than for the ground waves from train traffic.

3. BEAM SEPARATION EFFECTS

3.1 The Computational Model

To calculate the beam separations produced in the Superconducting Super Collider by ground waves, the closed-orbit effects due to the motion of each quadrupole in the complete lattice (September 1987 version³) were computed and summed, including the contributions from the eight straight sections. The SSC site, however, was modeled simply as a uniform, homogeneous, semi-infinite block of Austin chalk. The source of the ground waves for the blast case was a single point source vibrating on the surface at the quarry site. The train

model consisted of 48 such vibrating points with random phases over a length of 960 meters along the railroad that crosses over the northwest section of the ring, where the tunnel is the closest to the surface (20 meters) and where the largest ground vibrations were measured at tunnel depth. At each frequency of interest the amplitudes of the ground waves were computed at a measuring site as well as at the positions of all the quadrupoles. From these amplitudes the beam separations at the four crossing points per unit displacement at the measuring site were calculated.

The computer model and its mathematical treatment were described in the appendix of Reference 1. Using elastic constants of 18×10^9 newtons/m² (2.6×10^6 psi) in compression and 6×10^9 newtons/m² (8.7×10^5 psi) in shear, a Poisson ratio of 0.25, and a specific gravity of 2.0 for the Austin chalk gave compressional, shear, and Rayleigh (surface) wave velocities of 3.0, 1.73, and 1.59 km/sec, respectively.

This model of the site and the mathematical treatment used for the ground-wave propagation are, of course, much too simple to be trusted in detail. However, since the model was normalized to the amplitudes and frequency spectra measured by the Hennons² at the proper tunnel depths, we feel that the calculations of the resultant beam separations should be of the correct order of magnitude. More complete measurements in the actual tunnel with the final quadrupole magnet assemblies will, of course, be necessary.

3.2 Beam Separation due to Train Traffic

3.2.1 Simulation Results. The beam separations at the crossing points in the SSC produced by train-induced ground vibrations vary considerably with the wavelength of the vibration, the position of the railroad crossing relative to the FODO lattice in the arcs, and the attenuation encountered by the waves. These features involve interference effects between the closed-orbit contributions produced by the many quadrupoles. The arc regions of the lattice dominate these effects, rather than the "high-beta" interaction regions, because the important

railroad crossings occur in the arcs. Because of the repeating FODO lattice structure in the arcs, the beam separation effects have maxima where the ground wavelength is equal to the average betatron wavelength (about 900 meters in the 1987 lattice model used here, but 710 meters in the 1989 lattice), and at 1/3 and 1/5 of the betatron wavelength. For the Rayleigh (surface) wave velocity used in the computational model (1.59 km/sec), the corresponding ground-wave frequencies are 1.8, 5.4, and 8.8 Hz.

Figure 8 shows the calculated beam separation at the two low-beta crossings in the SSC versus the frequency of the train-induced ground wave for a characteristic attenuation length of 10 km/Hz. The force function used to simulate crudely the train effects was flat from 0 to 5 Hz and then dropped with a Gaussian exponential with an rms width of 4 Hz. Its amplitude was adjusted to produce a vertical displacement of about 0.5 micron at a frequency of 2 Hz at tunnel depth at the A measuring site (Figure 1) when a characteristic attenuation length of 0.4 km/Hz was applied.

The beam separation at the two low-beta ($\beta^* = 0.5$ meter) crossings show quite clearly the interference maxima that can occur when the ground wavelength is equal to the betatron wavelength and when it is equal to 1/3 and 1/5 of the betatron wavelength (1.8, 5.4, and 8.8 Hz, respectively).

The separation spectra for the two crossings differ both in magnitude and in shape. Recall that the closed-orbit at point s [$y_{co}(s)$] produced by the motion δy of one quadrupole with focal length f_q is

$$y_{co}(s) = \delta y \cos[\Phi(s) - \pi Q]/2f_q \sin \pi Q,$$

where Q is the betatron frequency in the y -plane, and $\Phi(s)$ is the betatron phase difference between the quadrupole and the point s . The differences between the two spectra of Figure 8 are due partly to the betatron phase difference between the two crossings, which is an odd multiple of 90 degrees, and partly to the

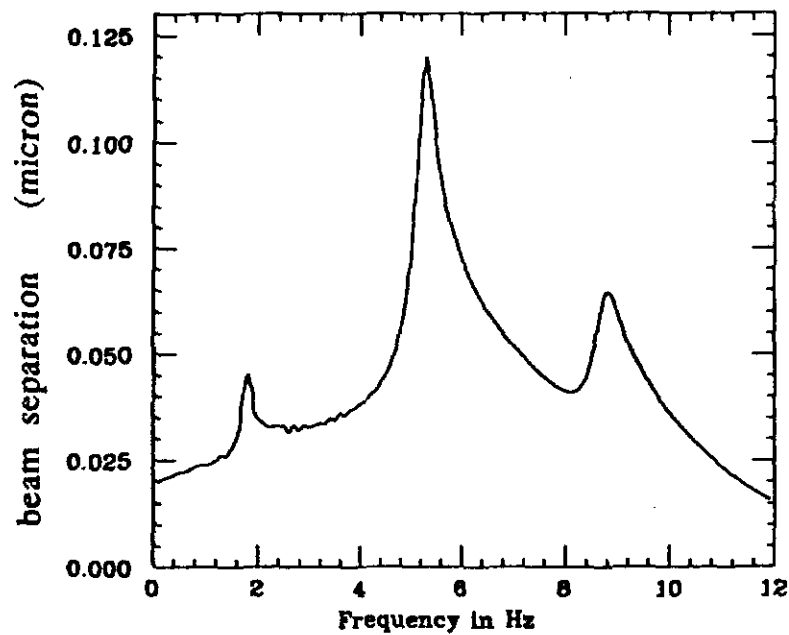
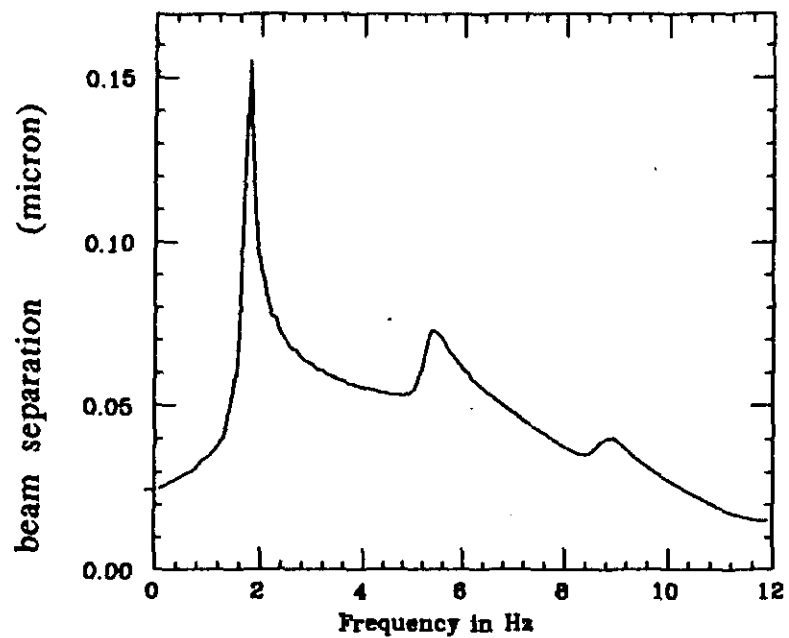


Figure 8. The Beam Separation Spectra at the Two Low-beta Crossings Versus Frequency of the Train Vibrations for a Characteristic Attenuation Length of 10 km/Hz.

variation with frequency of the phase difference between each crossing and the effective center of the closed-orbit disturbance.

Figure 9 shows the variation of the beam-separation spectrum at one of the low-beta crossings with the value of the characteristic attenuation length. As the ground becomes more absorptive, fewer quadrupoles are effective in producing the total closed orbit, so that interference effects become much less pronounced.

The beam-separation spectra vary also with the position of the railroad crossing along the arc in a complicated manner. Figure 10 shows the variation of the beam separation at the two low-beta crossings with position of the overhead railroad crossing along the 90-degree FODO lattice for the case of a 1 km/Hz attenuation length and at a vibration frequency of 2 Hz. Figure 11 shows the same case but at a frequency of 8 Hz. Similarly, Figure 12 shows the variation for the case of a 10 km/Hz characteristic attenuation length and a frequency of 2 Hz, and Figure 13 for the case of 10 km/Hz and 8 Hz. It has been noted that in each of the four figures the curves for the two crossing points are identical except for relative shift of 90 degrees and that they repeat at 180-degree intervals along the arc, as expected for this lattice configuration, since only the absolute values of the beam separations are calculated. It has also been noted for some vibration frequencies and some values of the characteristic attenuation length that the separation maxima occur when the train crossing is directly above a focussing quad (in the upper ring), and in other cases when it is above a defocussing quad, and in some cases when it is in between. Consequently, it is difficult to choose the optimum position of the lattice relative to the railroad crossing.

The same calculations were carried out for the beam separations at the medium-beta ($\beta^* = 10$ meters) crossings. As expected, the maximum separations scale simply with $\sqrt{\beta^*}$. Thus, in units of beam width, the maximum separations at the low- and medium-beta crossings are the same.

3.2.2 Beam Separation in the SSC due to Train Traffic—Worst Case. The largest recorded geophone signal from a train crossing over the SSC ring cor-

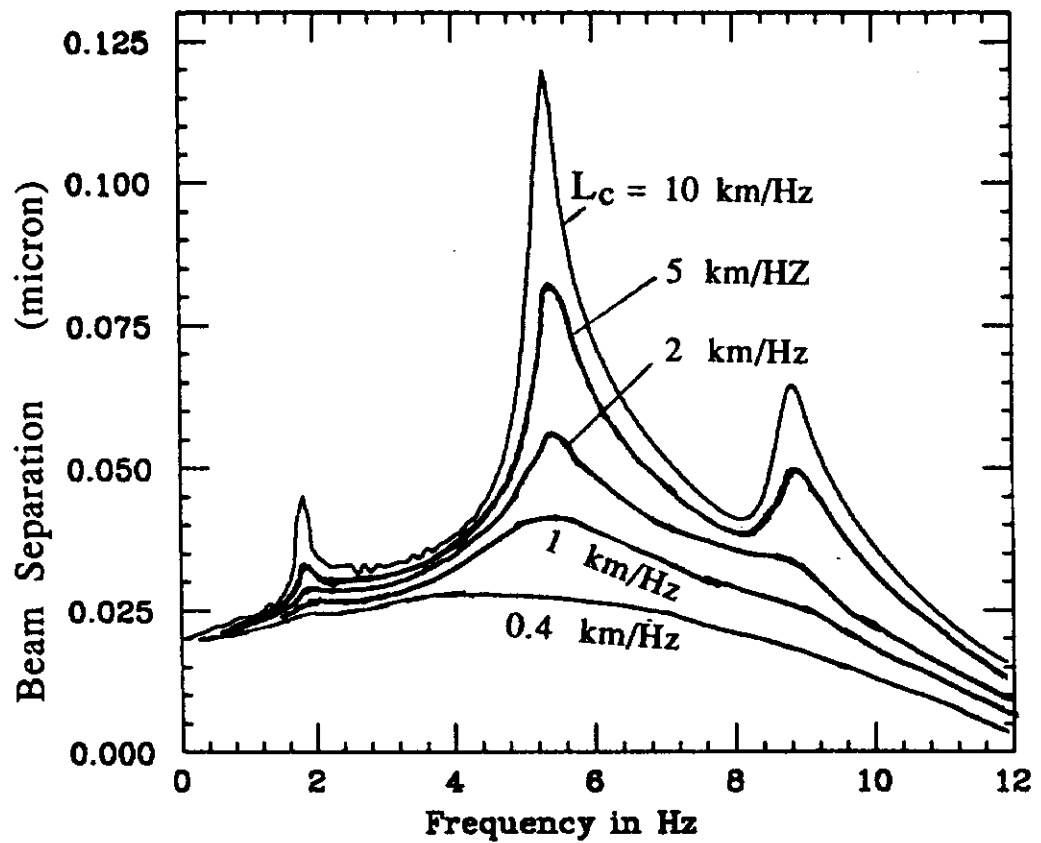


Figure 9. The Variation of the Beam-separation Spectrum due to a Train Crossing with the Value of the Characteristic Attenuation Length.

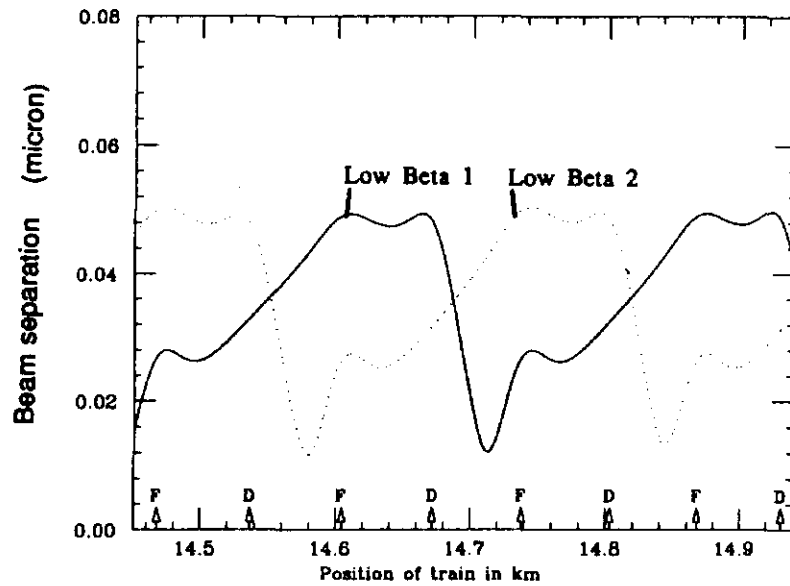


Figure 10. The Variation of the Beam Separation at the Two Low-beta Crossings at a Vibration Frequency of 2 Hz Versus Position of the Overhead Railroad Crossing Along the Arc, with a Characteristic Attenuation Length of 1 km/Hz. Positions of the focusing (F) and defocussing (D) quadrupole magnets in the upper ring are indicated. The half-cell length is 114.25 meters. The phase shift per cell is 90° .

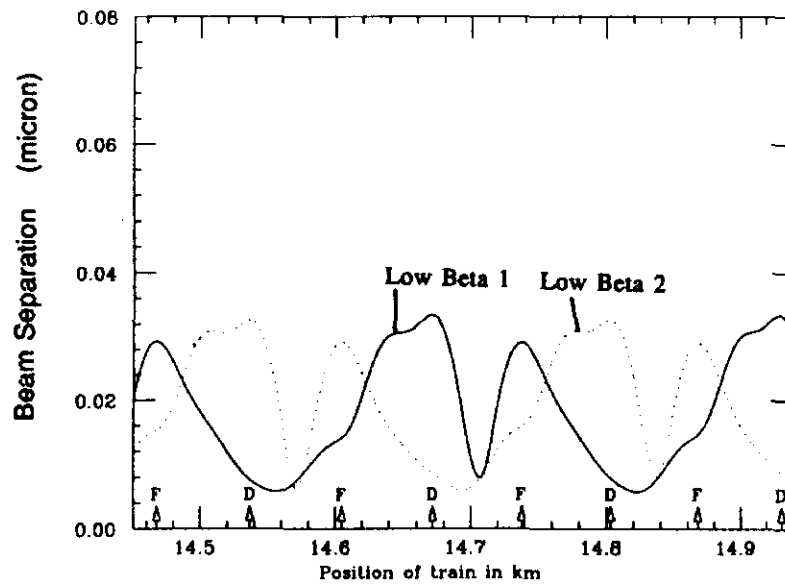


Figure 11. The Similar Variation of the Beam Separation at 8 Hz.

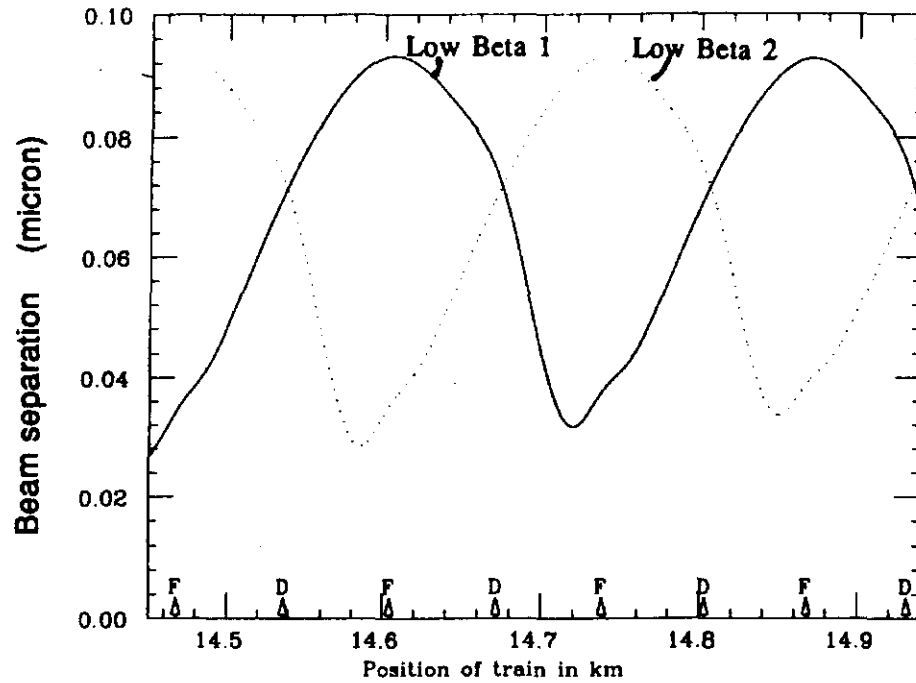


Figure 12. Variation of the Two Low-beta Beam Separations at 2Hz Versus Position to the Overhead Railroad Crossing, with a Characteristic Attenuation Length of 10 km/Hz.

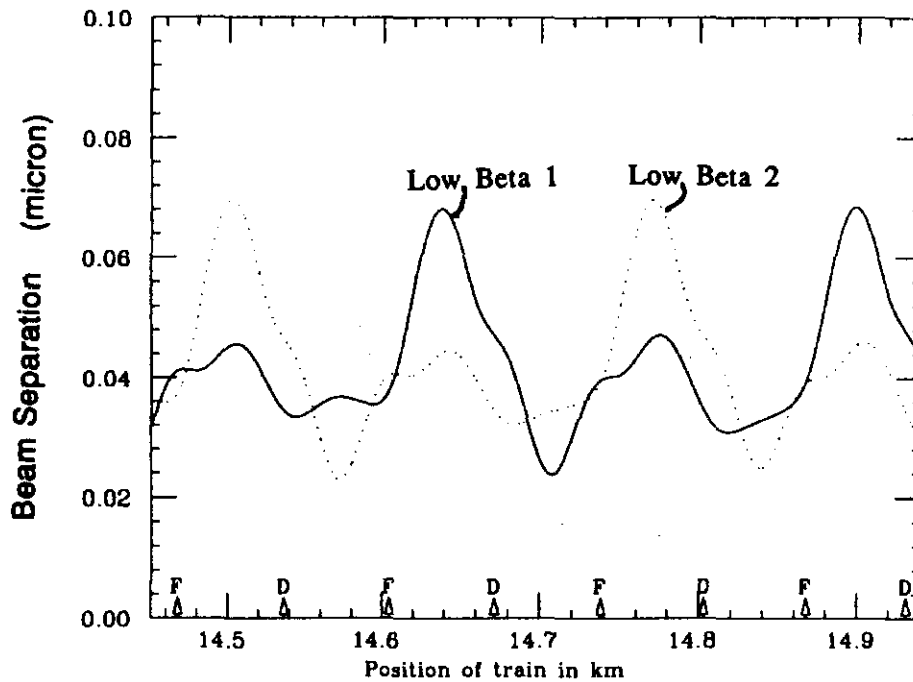


Figure 13. The Similar Variation at a Vibration Frequency of 8 Hz.

responded to a peak vertical displacement at tunnel depth of 0.55 micron at a frequency of about 3 Hz plus a broad maximum of 0.58 micron amplitude at about 7 Hz, as discussed in *Measured Ground-Wave Displacements*. Since the frequency spectrum of the ground waves from a train can vary with train speed and other conditions, and since the measured wave velocities at the site varied over a wide range (see Table 1), in order to evaluate the worst case for the SSC, we assumed that the “3-Hz” amplitude was at the betatron wavelength (1.8 Hz in the 1987 lattice used in the simulation, but 2.3 Hz if the 1989 lattice had been used) and that the broad “7-Hz” maximum was half at the $\lambda_\beta/3$ (5.4 Hz) and half at the $\lambda_\beta/5$ (8.8 Hz) resonances. We assumed also at each frequency and attenuation factor that the position of the train crossing was such as to maximize the separation at one of the beam crossings. The maximum separation expected at one of the low-beta crossings is obtained then by multiplying the measured vertical displacement at the measuring Site A by the maximum calculated beam separation per unit displacement at the A site for each frequency component and attenuation constant of interest. The results are listed in Table 2. The total maximum separations are given both in microns (μ) and in rms beam widths (σ). The nominal rms beam width at $\beta^* = 0.5$ m is 4.8 microns.

Thus, this estimate of the maximum beam separation at a low-beta interaction point due to a train crossing over the northwest arc of the SSC is about

Table 2. Maximum Beam Separation at a Low-Beta Crossing due to a Train—Worst Case

Measured at Site A				Calc. Separ/ δz_A			Separation at Low-Beta			
δz_1 at f_1		δz_2 at f_2		L_c	at f_1	at f_2	due to f_1	due to f_2	total	
μ	Hz	μ	Hz	Hz	μ/μ	μ/μ	μ	μ	μ	σ
0.55	3	0.58	7	1	.091	.072	.050	.042	.092	.019
0.55	3	0.58	7	2	.123	.081	.068	.047	.115	.024
0.55	3	0.58	7	5	.188	.115	.103	.066	.169	.035

0.092 micron, or 1.9 per cent of the rms beam width, if the effective characteristic attenuation length is 1 km/Hz, and 0.169 micron, or 3.5 per cent of the rms beam width, if it is 5 km/Hz. It must be remembered that amplification of the ground wave amplitude can occur due to the magnet supports. The HERA superconducting quadrupole supports⁴, for example, have been found to have amplification factors in the range of 2 to 4.

The variation of luminosity \mathcal{L} with beam separation D is given⁵ by

$$\mathcal{L} = \mathcal{L}_o \exp -(D/2\sigma)^2$$

where \mathcal{L}_o is the luminosity when the beams are well centered. If we assume that the separations given in Table 2 are increased by a factor of 5 due to magnet-support amplification, then the drop in luminosity in the worst case is only about 0.8%.

3.3 Beam Separation due to Quarry Blasts

3.3.1 Simulation Results. The quarry blast was simulated as a vibrating point at the known quarry coordinates near Midlothian, 9.4 km to the northwest of the measuring site A in the northwest section of the ring. As in the previous case of the train vibrations, the beam separations at the four interaction points per unit displacement at measuring site A were calculated from the computed displacements all around the ring. These computations were carried out at frequencies up to 6 Hz, the measured range of interest.

The computed beam-separation spectra at the two low-beta crossings for a characteristic attenuation length of 10 km/Hz are shown in Figure 14. The response of the system at low frequencies is relatively small until the ground wavelength approaches the average betatron wavelength (at 1.8 Hz). These spectra were found not to change significantly when the quarry site was moved by 200 meters in any direction.

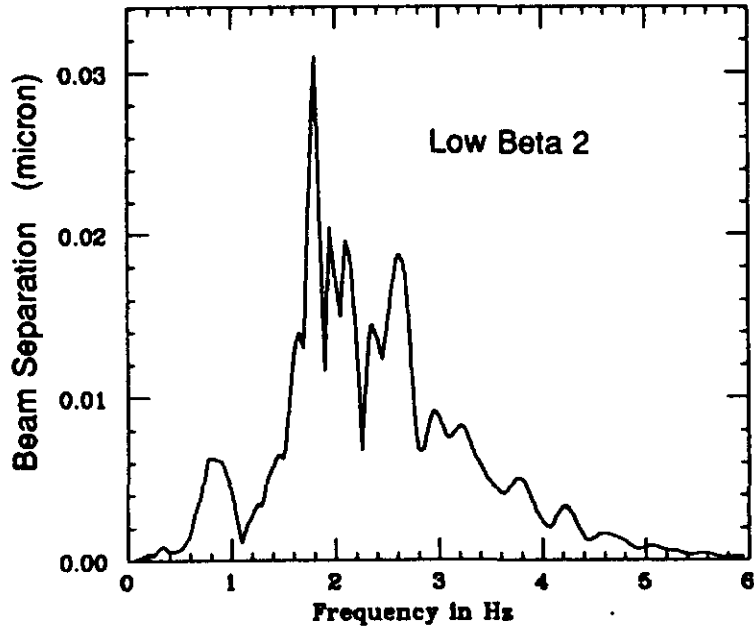
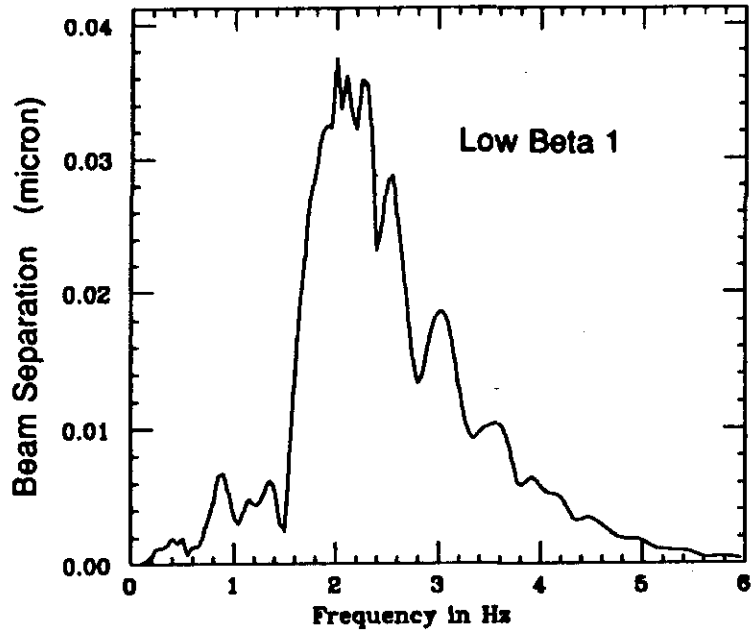


Figure 14. Computed Beam Separation Spectra at the Two Low-beta Crossings due to a Point Source at the Quarry Location, with a Characteristic Attenuation Length of 10 km/Hz.

The measured displacements at Site A due to the largest recorded blast was characterized as having one component with an amplitude of 1.4 micron near 1 Hz, and another of 1.1 micron near 3 Hz. Since the “1-Hz” peak in the measured displacement spectrum extends well into the sharp rise of the computed beam-separation spectrum and because also of the many uncertainties in the effective properties of the Austin chalk, we evaluated the beam separation due to this peak as if it were half at the frequency of 1 Hz and half at 2 Hz. The results are listed in Table 3.

Thus, the maximum beam separation at a low-beta crossing due to a quarry blast can be a significant fraction of the rms beam width. If, in addition we assume an amplification by a factor of 5 due to the quadrupole-magnet support structures, the maximum beam separation in Table 3 becomes 2.1 times the rms beam width, in which case the luminosity drops by 67%. Thus, the luminosity can be significantly reduced by a quarry blast for some tens-of-seconds if suitable compensation is not applied. Fortunately, the rate of quarry blasts is only about 2 or 3 per week, so that such a momentary drop in luminosity could be tolerable to the experiments in the interaction regions, if adequate warning of impending blasts were made available.

Table 3. Maximum Beam Separation at a Low-Beta Crossing due to the Largest Recorded Quarry Blast

Measured at Site A				Calc. Separ/ δz_A			Separation at Low-Beta			
δz_1 at f_1		δz_2 at f_2		L_c	at f_1	at f_2	due to f_1	due to f_2	total	
μ	Hz	μ	Hz	Hz	μ/μ	μ/μ	μ	μ	μ	σ
1.43	1	1.08	3	10	0.44	0.83	0.63	0.90	1.53	0.14
1.43	1	1.08	3	20	0.65	1.04	0.93	1.12	2.05	0.42

4. COMPENSATION OF BEAM SEPARATION

For compensating the transient beam separations at the interaction points, the automatic beam centering scheme outlined by Jostlein⁵ should be workable. In this scheme one beam is rotated at the crossing point with an amplitude b at an angular frequency ω considerably higher than the characteristic frequencies of the error separation D that you wish to correct. The geometry is shown in Figure 15. Jostlein shows for b and D much smaller than the rms beam width σ that the luminosity \mathcal{L} varies approximately as

$$\mathcal{L} = \mathcal{L}_o [1 + A \cos(\theta + \omega t)]$$

where \mathcal{L}_o is the luminosity of well-centered beams and the modulating amplitude A is given by

$$A = 2bD/(4\sigma^2 - b^2 - D^2) \approx bD/2\sigma^2.$$

Thus a measurement of A gives the magnitude of the static or slowly varying separation D , and a Fourier analysis yields its direction θ .

Jostlein points out that the minimum detectable offset D_{\min} , as limited by statistical errors, is

$$D_{\min} = 4\sigma^2/[b\sqrt{(2M)}]$$

where M is the total number of counts recorded. Thus, to detect a separation of, say, $D = 0.45\sigma$ (which will cause a 5% drop in luminosity), the rotation amplitude b must be at least $6.3\sigma/\sqrt{M}$. In order that the rotation amplitude not cause appreciable loss in luminosity, b should be less than 0.2σ . The corresponding minimum number of total counts then is $M_{\min} \approx 10^3$. This requirement is easily satisfied, since at luminosity of $10^{33} \text{ cm}^{-2}\text{sec}^{-1}$, a p-p inelastic cross section of 100 millibarns, and a detection efficiency of 0.5, the counting rate is $5 \times 10^7 \text{ sec}^{-1}$.

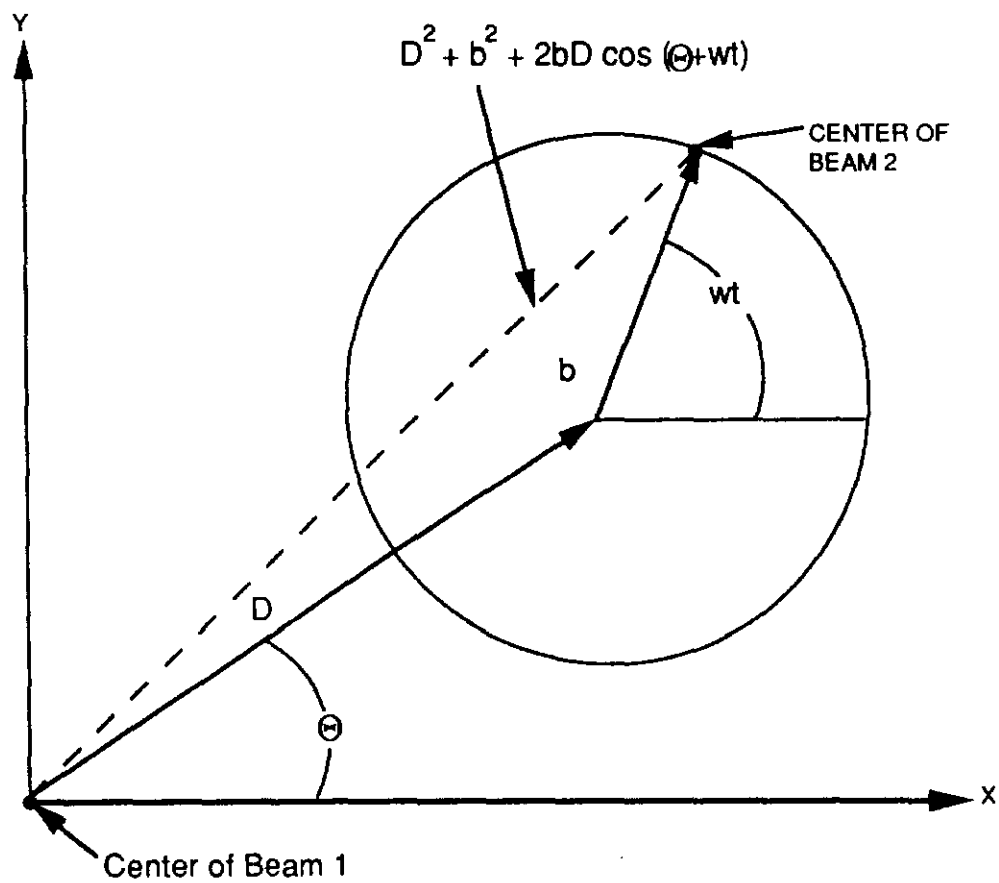


Figure 15. Geometry of the Beam-centering Scheme. The center of beam 1 is at the origin. Beam 2 has a misalignment D at the angle θ , which is to be determined. The center of beam 2 is made to follow a circle of radius b with angular frequency $\omega/2\pi$.

The frequency of rotation has thus far not entered into these considerations. The only requirement at this point is that the rotation period and the counting period should be short relative to the characteristic periods in the frequency spectrum of the separation D . However, observations of emittance growth⁶ when the transverse motion of one of two colliding beams is modulated indicate that the amplitude and the frequency of the rotated beam in the Jostlein scheme will have to be limited in order to avoid undue emittance growth. This subject is being studied and will be reported in a separate paper.

REFERENCES

1. K.Y. Ng and J.M. Peterson, *Ground-Motion Effects on the SSC*, Superconducting Super Collider Publication No. SSC-212 (Rev), Fermi National Accelerator Laboratory Publication No. FN-511 (Rev), revised January, 1990.
2. K. & D. Hennon, Earth Technology Corporation, *Field Measurements and Analyses of Underground Vibrations at the SSC Site*, Superconducting Super Collider Publication No. SSC-SR-1043, (December 1989).
3. A.A. Garren and D.E. Johnson, *The 90° (September 1987) SSC Lattice*, Superconducting Super Collider Publication No. SSC-146, (September 1987).
4. J. Rossbach, *Fast Ground Motion at HERA*, DESY 89-023, (February 1989).
5. H. Jostlein, *Automatic Beam Centering at the SSC Interaction Regions*, Fermi National Accelerator Laboratory Report No. TM-1253, (March 1984).
6. K. Cornelis, M. Meddahi, R. Schmidt, and D. Vanderplassche, *Experimental Study of a Beam Excitation in the Presence of the Beam-Beam Interaction*, SPS/AMS/Note 89-04, (January 1989).